Earth and Space Science

TECHNICAL REPORTS: DATA
10.1029/2019EA001024

Projecting Changes in Mean and Extreme Precipitation Over Eastern China During 2041–2060

Guangtao Dong[1,2], Zhiyu Jiang[1,3], Zhan Tian[4], Erasmo Buonomo[5], Laixiang Sun[6,7], and Dongli Fan[3]

[1]Shanghai Climate Center, Shanghai, China, [2]Key Laboratory of Cities' Mitigation and Adaptation to Climate Change in Shanghai, China Meteorological Administration, Shanghai, China, [3]Shanghai Institute of Technology, Shanghai, China, [4]School of Environmental Science and Engineering, Southern University of Science and Technology, Shenzhen, China, [5]Met Office Hadley Centre, Exeter, UK, [6]Department of Geographical Sciences, University of Maryland, College Park, MD, USA, [7]School of Finance and Management, SOAS University of London, London, UK

Abstract This report summarizes the preliminary analysis of the PRECIS 2.0 simulation results, with an emphasis on the priority concerns of Shanghai municipal government and other local governments in the Yangtze River Delta (YRD) Region, and research gaps in the literature. This study employs two regional climate models (RCMs) that are the Providing REgional Climate Impacts for Studies (PRECIS) and Weather Research and Forecasting (WRF), being driven by HadGEM2-ES and IPSL-CM5A, two global circulation models (GCMs) from the Coupled Model Intercomparison Project Phase 5 (CMIP5), to investigate the impact of global warming on the characteristics of mean and extreme precipitation over Eastern China. The capacity of two RCMs and its driving GCMs in reproducing the historical climate during the baseline period (1981–2000) are first evaluated, and then the projections of mean and extreme precipitation over future warming climate period (2041–2060) under the scenarios of the Representative Concentration Pathways (RCPs) 4.5 and 8.5 are carried out. Our analysis shows that with the improved resolution and better representation of finer-scale physical processes, WRF and PRECIS downscaling displays obvious advantages over their driving GCMs (IPSL and HadGEM, respectively) in the validation runs. In particular, the two RCMs are able to capture the observed features of spatial distributions of extreme precipitation indices including V95p, R95t, and SDII. The future projections indicate that increased radiative forcing from RCP4.5 to RCP8.5 emission scenarios would add further strength to the daily precipitation intensity by 2041–2060.

Key Points:
- This report presents projections of changes in mean and extreme precipitation over Eastern China for the middle of the 21st century
- We use two regional climate models driven by two global circulation models to reduce the modeling uncertainty

Supporting Information:
- Supporting Information S1

Correspondence to:
Z. Tian and L. Sun,
tianz@sustech.edu.cn;
ls28@soas.ac.uk;
lsun123@umd.edu

Citation:
Dong, G., Jiang, Z., Tian, Z., Buonomo, E., Sun, L., & Fan, D. (2020). Projecting changes in mean and extreme precipitation over eastern China during 2041–2060. *Earth and Space Science*, *7*, e2019EA001024. https://doi.org/10.1029/2019EA001024

Received 13 DEC 2019
Accepted 27 JUL 2020
Accepted article online 30 JUL 2020

1. Introduction

Climate extremes studies have drawn increasing concerns in recent years owing to the server impacts of extreme climate events on social stability, economic activities, lives, property, and natural ecosystems (Easterling et al., 2000; Ghosh et al., 2019; IPCC, 2012; Liu et al., 2012; Moore et al., 2015; Shivam et al., 2017; Wang et al., 2012; Wu et al., 2019; Zhai et al., 2005). Precipitation extremes that caused natural hazards, such as floods and droughts, are expected to occur more frequently with increasing intensity in the warming world, leading to more server damage to infrastructure and ecology, life, and agriculture if effective mitigation measures are absent (Fu et al., 2010; Liang et al., 2019; Marengo et al., 2011; Penalba & Robledo, 2010; Zhang et al., 2010). Numerous studies have focused on the trends in extreme precipitation events in China based on observed daily precipitation and indicated the increasing trends in frequency and intensity (Duan et al., 2019; Ge et al., 2019; Gemmer et al., 2011; Ma et al., 2015; Sun & Ao, 2013; Yang et al., 2010; You et al., 2011). In addition, the damages caused by extreme precipitation events are regional and/or local. It has become a high priority for climate services to detect the significant changes in the frequency and intensity of extreme precipitation using historical data records and also to produce the reliable future projections of extreme precipitation indicators and thresholds on regional and local scales based on climate models.

Coupled global circulation models (GCMs) forced by the climate scenarios of the Representative Concentration Pathways (RCPs) within the CMIP5 (Coupled Model Intercomparison Project Phase 5) are the state-of-the-art GCMs and the useful tools for estimating trends and variabilities of future climate and extremes, and for evaluating future climate change under various RCP scenarios. Based on the results of CMIP5-GCMs simulations, several studies have presented the changes in extreme precipitation events over different regions under different RCP scenarios (Chen, 2013; Chen et al., 2015; Jiang et al., 2015;

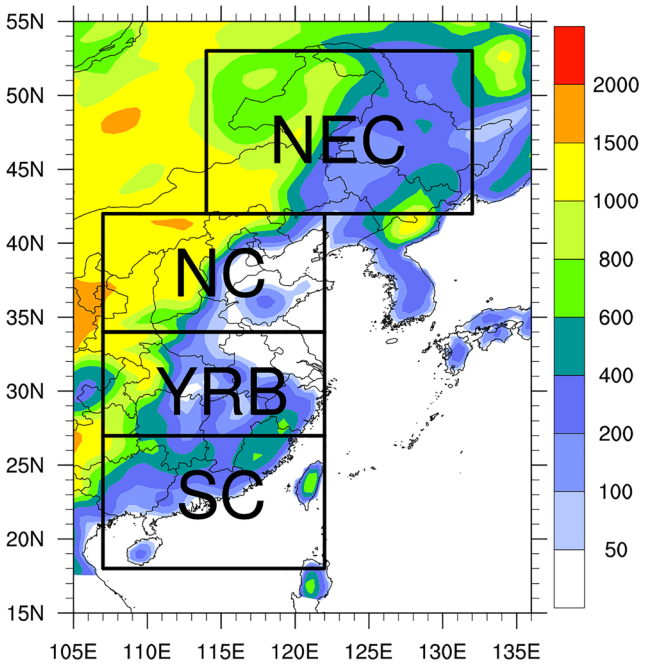

Figure 1. Study domain and four subregions in Eastern China: Northeast China (NEC, 114–132°E, 42–53°N); North China (NC, 107–122°E, 34°–42°N); Yangtze and Huai-He River Basin (YRB, 107–122°E, 27–34°N) and South China (SC, 107–122°E, 18–27°N).

Li et al., 2016; Sillmann, Kharin, Zhang, et al., 2013; Sillmann, Kharin, Zwiers, et al., 2013; Xu et al., 2019; Zhu et al., 2018). However, GCMs have difficulties in resolving mesoscale or regional scale climate features for their relatively coarse spatial resolution, particularly in projecting the precipitation extremes. And most of GCMs typically overestimate annual and summer precipitation in most areas of China (Bao & Feng, 2016; Chen & Frauenfeld, 2014; Wang et al., 2012).

Dynamic downscaling based on regional climate models (RCMs), which have high spatial resolution, finer surface parameters, and more complicated parameterization schemes, are widely adopted to study regional and local climate and extreme events (Bao et al., 2015; Bürger et al., 2013; Gao et al., 2012; Knutson et al., 2013; Pielke & Wilby, 2012; Singh et al., 2013; Tang et al., 2016; Yu et al., 2019; Zhai et al., 2005; Zou & Zhou et al., 2018; Zhou, 2013). Dynamic downscaling is of great predominance compared to GCM simulations in mean climate and extreme climate event and performs better over East Asia (Gao et al., 2002, 2008, 2012; Hui et al., 2018a; Lee et al., 2014; Park et al., 2016; Wang et al., 2012; Yu et al., 2014). Qin and Xie (2016) examined the frequency and intensity of precipitation extremes in China using RegCM4 forced by GCM GFDL_ESM2M, and their simulations were conducted under the middle emission scenario RCP4.5. It turned out that RegCM4 generally performed better in most river basins of China compared to GFDL in historical period, and relative to the historical period, more precipitation extremes will occur especially in Southeast China. Wang et al. (2012) reviewed recent studies of climate extremes with a focus on climatological features, variabilities, and trends in China based on observational data and simulations of global climate model and RCM. They pointed out that RCMs with higher resolutions often show predominance compared to GCM simulations and could improve the performance of simulations of precipitation extremes over China. Yu et al. (2014) described a dynamical downscaling simulation over China by nesting WRF into the Community Atmosphere Model (CAM) of the National Center for Atmospheric Research (NCAR). The results showed that dynamical downscaling is of great value in improving the model simulation of regional climatic characteristics.

In this study, we mainly focus on the following two areas. First, we evaluate the capability of four climate models in simulating mean and extreme precipitation for the reference period from 1981 to 2000 over Eastern China (the area in the east of the 107°E) and four subregions of Eastern China (Figure 1). The two RCMs we select are the Weather Research and Forecasting (WRF) model and Providing regional Climates for Impact Studies (PRECIS2.0) model, which are forced by the GCM IPSL-CM5A-LR and HadGEM2-ES, respectively. Second, we investigate the changes in precipitation extremes in future based on these four climate models for the period 2041–2060 under the RCP4.5 and RCP8.5 scenarios.

2. Data and Methods

The Eastern China region from 107°E to the eastern coast lines is divided into four subregions (Figure 1). The observation data used for model validation and reference are from the CN05.1 gridded data set (Wu & Gao, 2013). The data set is based on observation data from 2,416 meteorological stations in China with a horizontal resolution of 0.25° × 0.25° (longitude × latitude). The data set includes daily precipitation, daily average surface temperature, maximum temperature, minimum temperature, evaporation, average wind speed, relative humidity, and other meteorological variables from 1961 to 2012. At present, this data set is widely used in climate model validations (Gao et al., 2013; Hui et al., 2018a; Yu et al., 2014; Zhou et al., 2014).

In this study, IPSL-CM5A-LR and HadGEM2-ES models are adopted as initial and boundary conditions for WRF and PRECIS, respectively. The WRF model is a state-of-the-art mesoscale numerical weather prediction system designed to serve both operational forecasting and atmospheric research needs. PRECIS is a

Table 1
Information of the Climate Extreme Indices Analyzed in the Present Analysis

Index	Descriptive name	Definition	Units
PRCPTOT	Wet day precipitation	Annual total PRCP in wet days (RR > 1 mm)	mm
Wet days	Number of wet days	Annual total number of days when RR ≥ 1.0 mm	days
R10mm	Number of days with RR ≥ 10.0 mm	Annual total number of days with RR ≥ 10.0 mm	days
SDII	Simple daily intensity index	The total rainfall divided by the number of wet days in the year	mm day^{-1}
V95p	Extreme precipitation value	Value when RR > 95th percentile	mm
R95d	Days of Extreme precipitation	Annual total number of days when RR ≥ V95p	days
R95t	Heavy precipitation fraction	Fraction of annual total precipitation events exceeding the 1981–2000 95th percentile	%
Rx5day	Maximum precipitation on 5 consecutive days	Maximum amount of precipitation on five consecutive days in a year	mm
CDD	Consecutive dry days	Maximum number of consecutive days without precipitation in the year	days

Notes: RR means daily precipitation.

regional climate modeling system developed at the Met Office Hadley Centre, UK, and has been widely applied in regional simulations (Feng et al., 2012; Wang et al., 2014, 2015). Two RCMs are run over East Asia with all of China included, with a same horizontal resolution of 50 km. WRF takes 102 (latitude) × 116 (longitude) grid points, while PRECIS2.0 takes 183 (latitude) × 219 (longitude) grid points. RCMs are integrated for 20 years both in the reference period from 1981 to 2000 and the future period from 2041 to 2060 under both the middle- and high-emission scenarios RCP4.5 and RCP8.5.

The precipitation extreme indices used in this study are adopted from ETCCDI (Expert Team on Climate Change Detection and Indices, http://cccma.seos.uvic.ca/ETCCDI). These indices have been widely used in characterizing precipitation extremes (Li et al., 2018; Qin & Xie, 2016; Sillmann, Kharin, Zhang, et al., 2013; Sillmann, Kharin, Zwiers, et al., 2013; You et al., 2011). We employ a set of five precipitation indices from ETCCDI, and other four custom indices including the number of wet days, V95p, R95d, and R95t (Table 1). These indices are calculated in each station and model's grid, and then the results of these indices are interpolated to a common 0.5° × 0.5° grid using a bilinear interpolation scheme.

3. Model Evaluation

In this section, we quantitatively evaluate the performance of individual climate models based on observations over Eastern China.

First, we examine the ability of the four climate models in reproducing the spatial distribution of extreme indices over Eastern China. Figures 2 and 3 exhibit the relative errors of four models for eight indices (PRCPTOT, wet days, R10mm, SDII, V95p, R95t, Rx5day, and CDD) in the period of 1981–2000. Results reveal that the spatial patterns of model biases vary substantially. For PRCPTOT, the annual average of observation (Figure 2a) shows that PRCPTOT increasing from the north to the south. IPSL-CM5A (Figure 2b) model exhibits underestimation in the south and overestimation in the north of Eastern China. The maximum relative error is more than 50% and mainly distribute in NEC subregion. Compared with IPSL-CM5A, WRF (Figure 2c) has weaken the biases obviously in the corresponding subregions, especially in NEC and SC subregions. Compare to IPSL-CM5A, HadGEM (Figure 2d) performs better in PRCPTOT with lower overestimation biases in the most area, especially in NEC, NC, and YRB subregions. However, the result of PRECIS2.0 simulation (Figure 2e) does not show evident improvements in comparison to that of HadGEM.

The IPSL model underestimates the annual precipitation in the middle and lower reaches of the Yangtze River Basin and the south area of the basin, and such biases are significantly reduced in WRF downscaling simulations. It may be attributed to a better representation of low-level water vapor flux and vorticity in WRF. In NE, the GCMs and RCMs all overestimate the precipitation because of the positive bias of low-level potential vorticity in RCMs and their forcing GCMs. Due to the larger overestimation of IPSL-CM5A, the improvements of the WRF over IPSL-CM5A are larger than that of PRECIS over HadGEM.

Obviously, the number of wet days is generally overestimated by each model. Figures 2g and 2i show that the overestimations of both GCMs are large, exceeding 60% in most area of Eastern China. Both RCMs

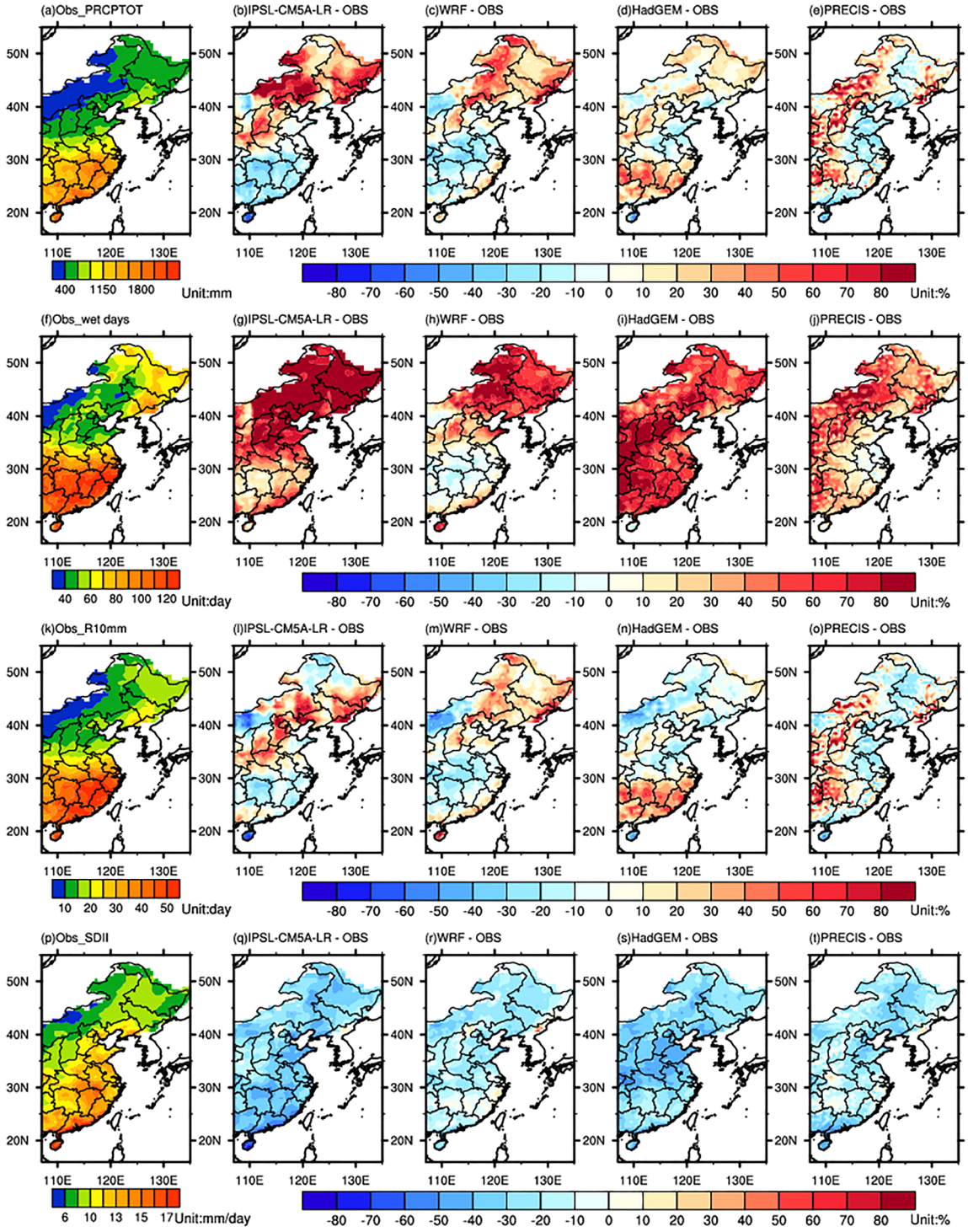

Figure 2. The spatial distribution of the annual average of observations and the relative bias ratio (%) of each model's simulation with reference to the observations for indices of PRCPTOT (a–e), number of wet days (f–j), R10mm (k–o), and SDII (p–t) over eastern China in 1981–2000.

(Figures 2h and 2j) show an improvement in simulation results by different extents and WRF performs better than PRECIS2.0. Figure 2h shows that WRF reduces the relative error in most area of the study region with the biases being reduced to less than 10% in SC and YRB subregions. PRECIS2.0 (Figure 2j) also abates the biases across almost all Eastern China, and the area with less than 10% biases main located in Jiangsu, Anhui, Shanghai, and Zhejiang province. Please note that the overestimation of the annual number of wet

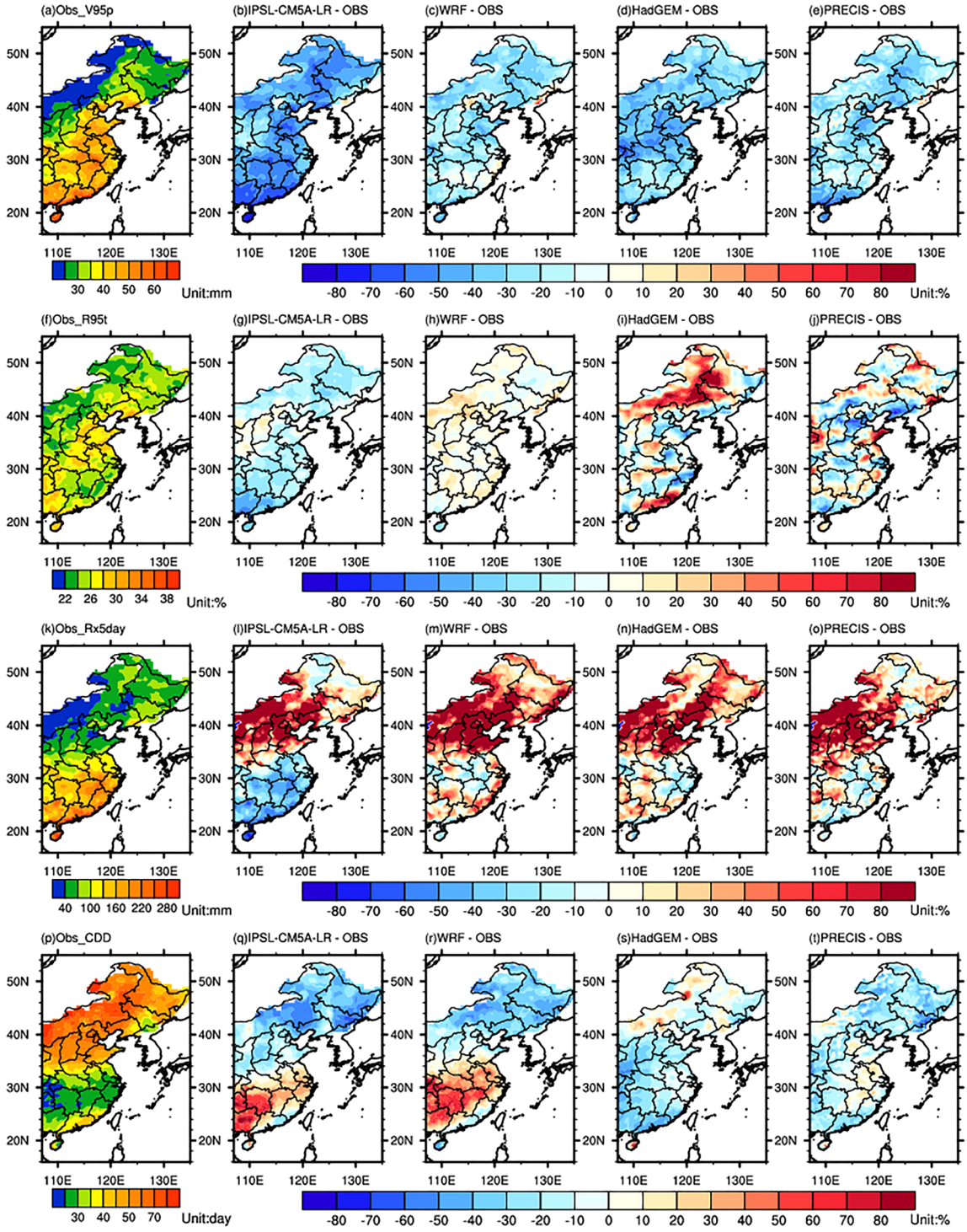

Figure 3. The spatial distribution of the annual average of observations and the relative bias ratio (%) of each model's simulation with reference to the observations for indices of V95p (a–e), R95t (f–j), Rx5day (k–o), and CDD (p–t).

days and the underestimation of the averaged daily precipitation intensity (SDII) have also been found with many other GCMs (e.g., Jiang et al., 2012; Xu et al., 2019). It is mainly due to the relatively lower resolution and deficiency in convection scheme (Chen & Gao, 2019). By contrast, with the higher resolution and much better representation of convection, most RCMs show significant improvements over their forcing GCMs in

simulating annual rainfall frequency and averaged daily precipitation intensity (Bao et al., 2015; Hui et al., 2018a; Zhu et al., 2018).

For R10mm, observations (Figure 2k) show a similar spatial distribution to that of PRCPTOT. IPSL simulations (Figure 2l) show an overestimation, locating mainly in NC and NEC subregions. WRF downscaling (Figure 2m) eliminates this overestimation by a certain extent. The PRECIS.0 (Figure 2o), by contrast, shows no significant improvement relative to HadGEM and the spatial pattern of its relative error is similarly to the index of PRCPTOT with different intensity.

For indices of SDII and V95p, the spatial distribution patterns of model biases are similar. The simulations of both GCMs and RCMs show a wide underestimation over Eastern China (Figures 2q–2t and Figures 3b–3e). WRF and PRECIS2.0 produce an obvious improvement in simulation results compared to IPSL and HadGEM respectively, and the biases in some subregion are reduced to less than 10%, even though there exits much underestimation over the study area.

For R95t, IPSL simulation results (Figure 3g) mainly show underestimation over most area of Eastern China, and the relative error in North China is less than 10%. The WRF simulation (Figure 3h) agrees with the observations better than IPSL with less than 10% biases over almost the whole area. HadGEM simulation results for R95t exhibit mixed positive biases and negative biases (Figure 3i), and PRECIS2.0 downscaling simulation results in less overestimated biases in NEC subregion (Figure 3j).

For Rx5day, IPSL (Figure 3l) produces underestimation in YRB and SC and overestimation in NC and NEC. The improvement on simulation results of WRF (Figure 3m) exists in partial area of YBR, reducing the biases to less than 10%. In SC, WRF simulation produces positive biases, contrary to the negative biases of IPSL, but with less magnitude. Similar to HadGEM (Figure 3n), PRECIS2.0 (Figure 3o) mainly performs an overestimation for Rx5day in most area and has reduced the biases by a certain extent in partial area of NEC.

For CDD, IPSL (Figure 3q) underestimates it mainly in NEC and NC and overestimates it in SC and YRB. The improving effect of WRF over IPSL (Figures 3r and 3t) is evident in NEC, although there still exist underestimated biases. But WRF simulation also shows an increase in the overestimated biases in SC and YRB compared to its driving model IPSL. Simulation results of HadGEM (Figure 3s) show an extent of biases within 10% in most area of NEC and underestimating biases in other subregions. Compared to HadGEM, PRECIS2.0 has better performance in part of the area of SC, YRB, and NC subregions in terms of lessening the underestimation biases, but deficient performance in NEC subregion in terms of increasing the underestimation biases. Because of their improved resolution and better representation of finer-scale physical processes, the two RCMs, that is, WRF and PRECIS downscaling, display obvious advantages over their driving GCMs (IPSL and HadGEM, respectively). They are able to capture the observed features of spatial distributions of extreme precipitation indices including V95p, R95t, and SDII and to exhibit higher spatial pattern correlations with the observations. Besides, the downscaling by RCMs presents more reasonable regional averages of extreme precipitation indices in most regions.

Of course, the performances of the two RCMs are not perfect, and there are still some biases in comparison with the observations. Part of the bias comes from the driving GCM, and part comes from the RCM itself. For example, the two GCMs overestimate the annual precipitation in the NEC region. As a result, the downscaling by the two RCMs also overestimate the annual precipitation over this region while the biases of RCMs are smaller than that of their forcing GCMs due to the better representation of low-level potential vorticity by the RCMs (Hui et al., 2018a). Meanwhile, the IPSL model underestimates the annual precipitation in the middle and lower reaches of the Yangtze River Basin, and also, in the south of the basin, such biases are significantly reduced in WRF downscaling simulations. WRF model even overestimates the annual precipitation in the southeast edge of China due to the positive vorticity anomalies over this region (Hui et al., 2018a).

The Taylor Diagram (Taylor, 2001) is used to summarize how closely the patterns of simulation results match the observations. The eight Taylor Diagrams in Figure 4 exhibit statistics of the eight extreme precipitation indices over Eastern China simulated by four climate models and verified against observations during 1981–2000. The statistics include the root-mean-square error (RMSE), the ratio of standardized deviations (SDs), and correlation coefficient (COR) between the observational pattern and simulated patterns. On the plot, the well simulated pattern with the low RMSE, low SD, and high COR will be closer to reference point marked "OBS." It is evident that two RCMs have better performance for PRCPTOT,

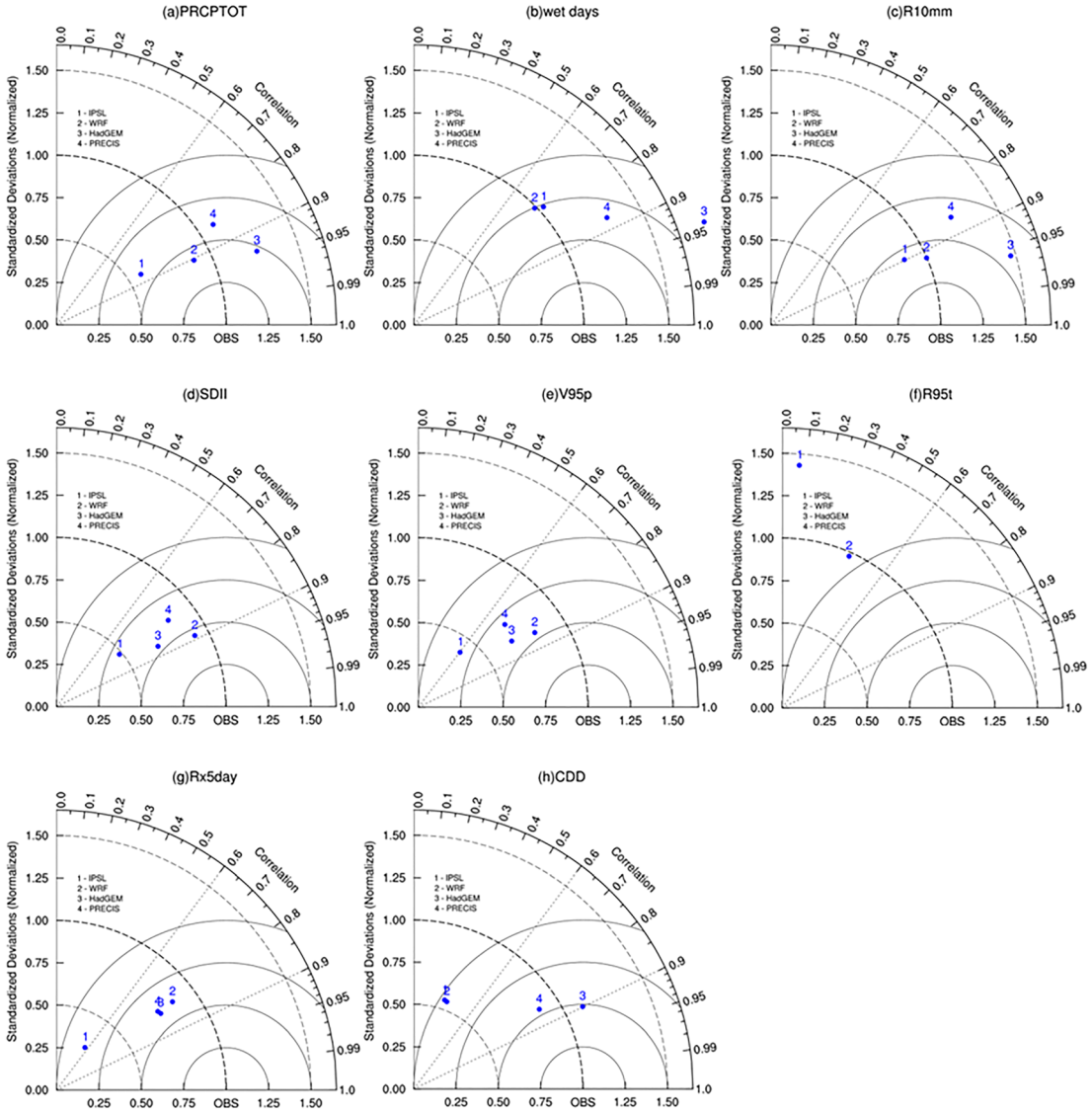

Figure 4. Taylor diagram displaying statistics of climatology of extreme precipitation indices over Eastern China simulated by four climate models (as numbered in the diagrams) and verified against observations during 1981–2000. The ordinate and abscissa are the ratio of the standard deviation of indices simulated by climate models with reference to observations. The angular axes show spatial correlations between simulations and observations. For the angular axes located between the two dotted lines, correlations are between 0.6 and 0.9.

number of wet days, R10mm, SDII, and V95p, in comparison to their driving GCMs in terms of the ratio of the standard deviation.

The simulated PRCPTOT and R10mm are similar across climate models. Though HadGEM has the highest COR, WRF has the best simulation capability according to the standard deviation. For R95t and Rx5day, WRF also has an improvement in the ratio of the standard deviation. In terms of spatial correlations, the performance of HadGEM on all indices is well with the exception of R95t compared to PRECIS2.0. WRF improves the spatial correlations between simulations and observations for indices PRCPTOT, R10mm, SDII, V95p, and Rx5day.

Although the RCM's downscaling skill is strongly limited by the skill of its driving GCM (Racherla et al., 2012), the performance of the two RCMs is dependent on geophysical locations, RCM applied, and extreme indices (Hui et al., 2018a; Yu et al., 2019). In terms of spatial correlation of whole Eastern China, WRF shows advantages in the representation of V95p, R95t, and SDII while PRECIS works better for the

Model_SubRegion	prcptot	wet days	R10mm	SDII	V95p	R95t	Rx5day	CDD
HadGEM_SC	22.27	69.45	32.45	-28.02	-28.76	-21.47	9.13	-31.66
HadGEM_YRB	13.98	72.94	18.6	-34.5	-38.09	-18.67	-3.27	-21.36
HadGEM_NC	4.55	73.24	-6.22	-39.72	-41.86	-25.35	65.88	-18.14
HadGEM_NEC	11.66	56.17	-5.85	-29.32	-30.79	-27.18	39.91	-2.68
PRECIS_SC	-1.33	35.93	3.63	-29	-36.44	-2.1	-3.17	-21.27
PRECIS_YRB	7.92	22.38	12.6	-13.59	-20.75	-5.69	4.15	-8.39
PRECIS_NC	9.81	40.4	5.67	-23	-26.94	-1.79	70.42	-13.94
PRECIS_NEC	13.41	47.13	-0.42	-24.31	-26.96	3.58	25.02	-25.48
IPSL_SC	-27.33	35.69	-7.87	-46.58	-63.16	-34.8	-46.89	24.66
IPSL_YRB	-15.78	31.6	-7.41	-35.61	-47.75	-17.73	-30.88	22.36
IPSL_NC	22.94	78.61	19.63	-32.12	-43.94	-5.27	58.18	-21.23
IPSL_NEC	44.7	114.49	15.7	-32.71	-47.62	-17.96	25.72	-40.89
WRF_SC	-1.92	14.66	6.07	-15.46	-21.47	2.06	15.85	16.01
WRF_YRB	-15.64	-3.73	-13.34	-13.83	-18.67	2.89	3.07	40.48
WRF_NC	3.21	28.55	2.07	-20.87	-25.35	7.1	84.14	-9.06
WRF_NEC	34.25	72.53	21.69	-22.43	-27.18	2.57	49.57	-37.51

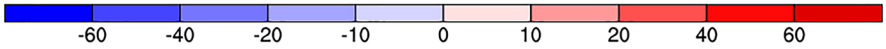

Figure 5. Regionally averaged bias of precipitation indices over four subregions simulated by the four climate models over 1981–2000 (units: %).

number of wet days and CDD. Meanwhile, WRF and PRECIS have nearly same ability in simulating annual precipitation amount, R10mm and RX5day.

In order to better grasp the biases of climate models in simulating the extreme precipitation indices, we have calculated the regional average relative error of the indices in four subregions (Figure 5). Figure 5 shows that all models present positive biases for the number of wet days except for WRF simulation in YRB and all models present negative biases for SDII and V95p in all subregions. For PRCPTOT and Rx5day, the four models generally exhibit overestimation. For CDD, simulations mainly exhibit negative biases, except for that IPSL and WRF produce positive biases in SC and YRB. PRCPTOT is generally overestimated, whereas R95t is generally underestimated, except for PRECIS2.0 in NEC and WRF in all four subregions.

Though biases are present in the simulations of the two RCMs, the absolute values of these biases are in general smaller than those of the driving GCMs. PRECIS2.0 has reduced the biases for the number of wet days, R10mm, and R95t in all subregions. WRF shows better performance for PRCPTOT, the number of wet days, SDII, and V95p. For PRCPTOT and R95t, the biases of both WRF and PRECIS2.0 are within 3% in SC. For other indices, only in a few subregions the two RCMs have higher biases compared to their driving GCMs. For example, HadGEM underestimates the CDD in the NEC by a margin of −2.68% on average, by contrast the corresponding average bias produced by PRECIS2.0 is −25.48%.

In conclusion, although the overestimated biases for PRCPTOT and the number of wet days and the underestimated biases for SDII, V95p, and CDD commonly exist in four subregions in the simulations of all four models, the two RCMs have better performance in general because they reduce the related biases by a meaningful margin in comparison with their driving GCMs. A comparison between WRF and PRECIS indicates that these two RCMs have different simulated capacities in different subregions. For example, although both WRF and PRECIS overestimate the annual precipitation (PRCPTOT) in NEC, the extent of overestimation by WRF is much larger than that by PRECIS. In NC region, PRECIS overestimates PRCPTOT by a moderate margin of 9.81% on average whereas the corresponding margin for WRF is even smaller, at 3.21%. Overall, WRF model shows better performance in NC and SC while PRECIS works better in NEC and YRB regions.

The summary validation assessment of the four models in Figure 5 shows a general overestimation of PRCPTOT and the number of wet days over all subregions. In order to uncover the temporal dynamics of such annual overestimation, we examine the ability of these four models in reproducing the monthly dynamics of precipitation and the number of wet days in the supporting information. Figures and discussions in the supporting information show that the four models are able to capture the annual cycle of

both precipitation and the number of wet days in subregions, especially in NC and NEC, with the two RCMs performing better than their driving GCMs.

4. Projections of the Extreme Climate Indices for the Middle of the 21st Century

The above analyses confirm that the four climate models, especially the two RCMs, do have a certain skill to simulate the key characteristics of observed extreme climate events in Eastern China. This validation supports our adoption of these four models for projecting extreme climate indices for the 21st century under selected emission scenarios. In this section we report the simulation results of these four climate models over the period of 2041–2060, which represents the middle of the 21st century, with reference to the baseline climate of 1981–2000.

Figures 6 and 7 present an overview of the projected changes of the eight precipitation extreme indices (PRCPTOT, wet days, R10mm, SDII, R95d, R95t, Rx5day, and CDD) over 2041–2060 under RCP4.5 scenario, relative to the baseline period of 1981–2000. For IPSL and WRF, large values of increase in PRCPTOT are shown in YRB, NC, and NEC (Figures 6a and 6b). HadGEM simulations project a general increase of PRCPTOT over Eastern China (Figure 6c). The PRECIS2.0 simulations project an increase of PRCPTOT value in YRB, NC, and NEC, while a decrease in SC (Figure 6d). As shown in Figures 6f and 6h, WRF and PRECIS simulations project a decrease in the number of wet days over SC and YRB. Similar results can be found in HadGEM simulations (Figure 6g). However, the IPSL simulations mainly present an increase in most areas (Figure 6e). The spatial patterns of changes in R10mm (Figures 6i–6) are similar to those of PRCPTOT (Figures 6a–6d), but with different extents of changes. For SDII, the four models all project an increase in almost all of study areas. However, in SC, both IPSL and WRF project a decrease by no more than 10% in most area of the region (Figures 6m and 6n), and in NEC, both HadGEM and PRECIS project a decrease by less than 10% (Figures 6m and 6n).

For R95d, WRF projects an increase over Eastern China, with the extent of increase in some areas exceeding 40% (Figure 7b). IPSL projects a greater increase than WRF in YRB, NC, and NEC, with the extent of increase in some areas exceeding 70% (Figure 7a). HadGEM also projects a larger increase of R95d in SC, YRB, and NC than PRECIS2.0 does (Figures 7c and 7d).

The spatial patterns of simulated changes in R95t are different across the four models (Figures 7e–7h). An increase is mainly distributed in NEC by IPSL and mainly distributed in SC and NEC by PRECIS2.0 (Figures 7e and 7h). The extent of increase in many parts of the study area exceeds 80%.

For Rx5day, IPSL and WRF produce similar features (Figures 7i and 7j). They both detect a general increase in NC and NEC, whereas a decrease in YRB. WRF produces greater increase than IPSL. HadGEM also projects an increase over most area (Figure 7k), and PRECIS projects mixed increases and decreases over Eastern China (Figure 7l). A comparison of spatial patterns of changes produced by the same model between R95d and Rx5day suggests that the changes of R95d and Rx5day are consistent. In particular, PRECIS produces highly similar patterns of changes (Figures 7d versus 7l).

For CDD, HadGEM projects a dominated decrease over the most area of the eastern China (Figure 7o), while IPSL projects an increase over the most area (Figure 7m). PRECIS2.0 projects increases in SC and decreases in NC and NEC (Figure 7p).

Figure 8 reports the projected changes of future precipitation under the RCP8.5 scenario from the baseline of 1981–2000 to the climate of 2041–2060. Under the RCP8.5 scenario, all four models project that annual precipitation over most of Eastern China will increase especially in NC and NEC (Figures 8a–8d). The magnitude of increase in northern areas is generally larger than that in the southern. This result is consistent with the result derived from RegCM4 driven by HadGEM2-ES that future precipitation will increase in China with larger increases in north than southern China (Shi et al., 2018). For the number of wet days, all four models project increases in north regions and decreases over south regions, with moderate margins of changes projected by WRF and PRECIS (Figures 8e–8h). The spatial distributions of changes in R10mm generally follow those of PRCPTOT (Figures 8i–8l), but with different magnitude. A general increase in SDII is projected by all four models except that IPSL and WRF project moderate decreases in and around Hunan province and in the northern part of NC (Figures 8m–8p). The spatial pattern of SDII projected by

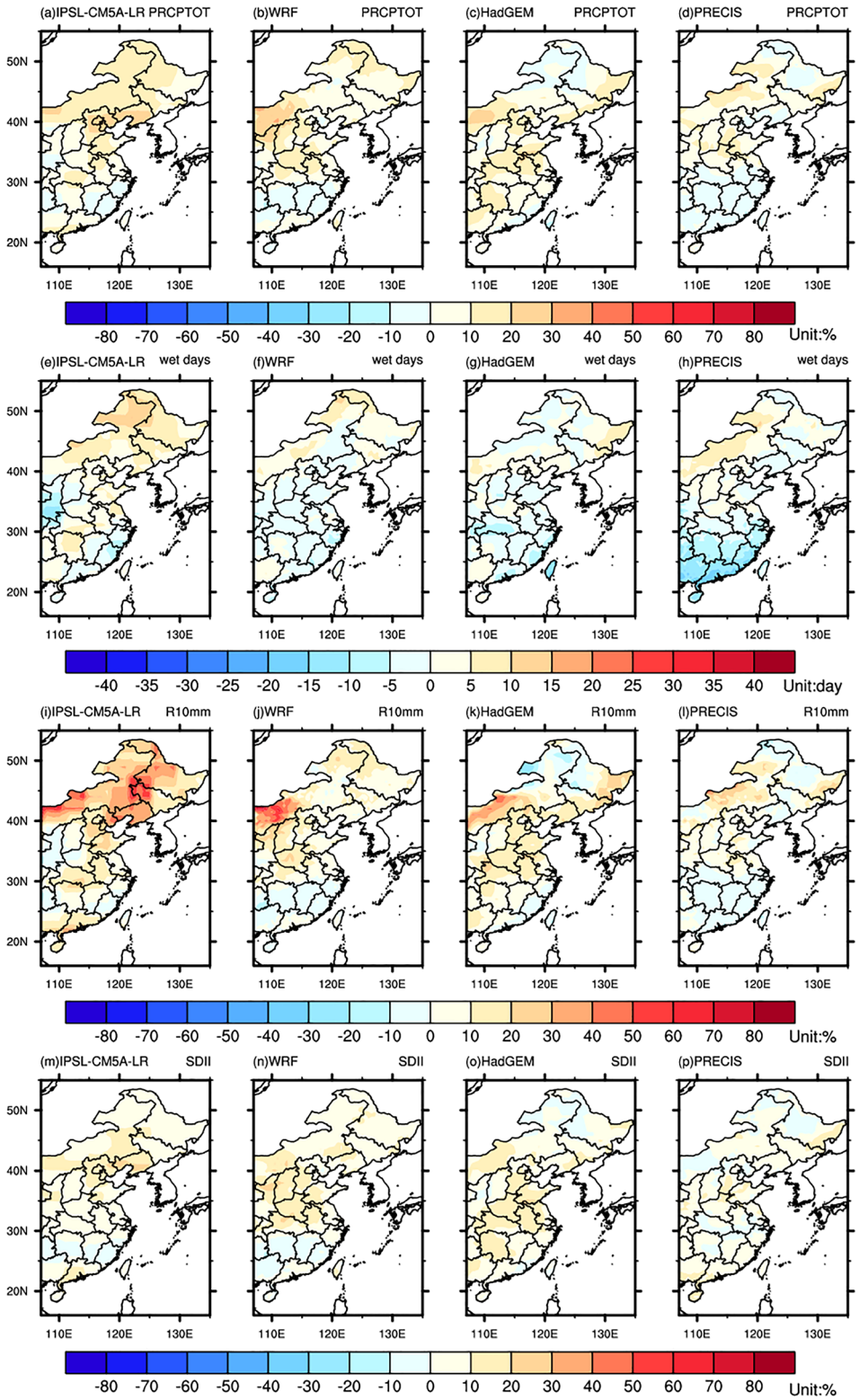

Figure 6. Changes in the annual mean state of precipitation indices between 2041–2060 and 1981–2000 under RCP4.5 scenario: PRCPTOT (a–d), number of wet days (e–h), R10mm (i–l), and SDII (m–p).

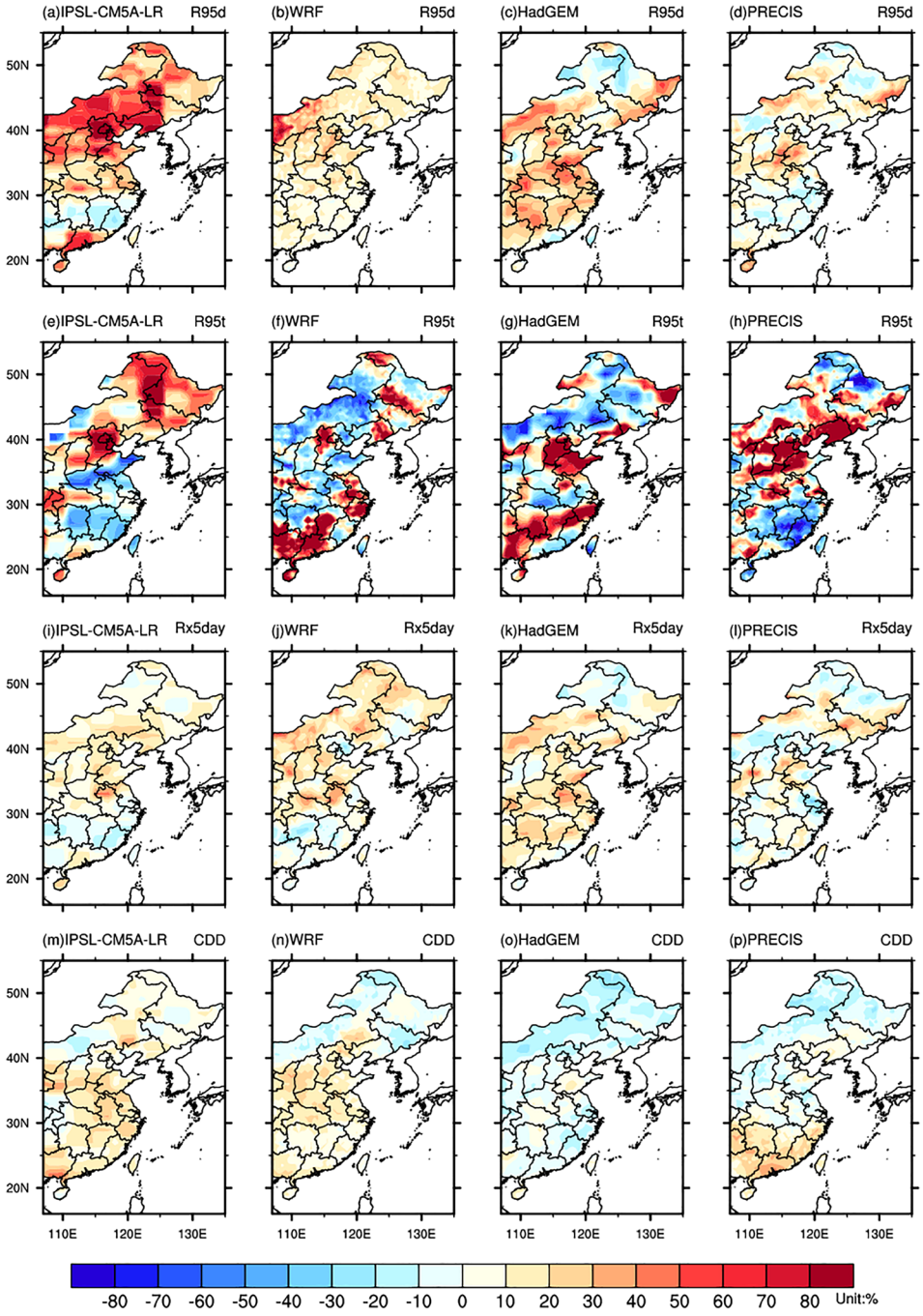

Figure 7. Changes in the annual mean state of precipitation indices between 2041–2060 and 1981–2000 under RCP4.5 scenario: R95d (a–d), R95t (e–h), Rx5day (i–l), and CDD (m–p).

PRECIS is similar to that in Zhu et al. (2018), which employs the same approach of PRECIS downscaling HadGEM2-ES during the 2050s.

Figure 9 presents the projected changes of extreme precipitation indices over Eastern China from the baseline to the climate of 2041–2060 under the RCP8.5 scenario. Under the RCP8.5 scenario, the four models all project an increase of R95d in most part of the study area (Figures 9a–9d). WRF and HadGEM project significant increase in NC, with the extent exceeding 50%. On the other hand, WRF and PRECIS project a decrease over some parts of SC. The spatial patterns of changes in R95t generally follow those in R95d if

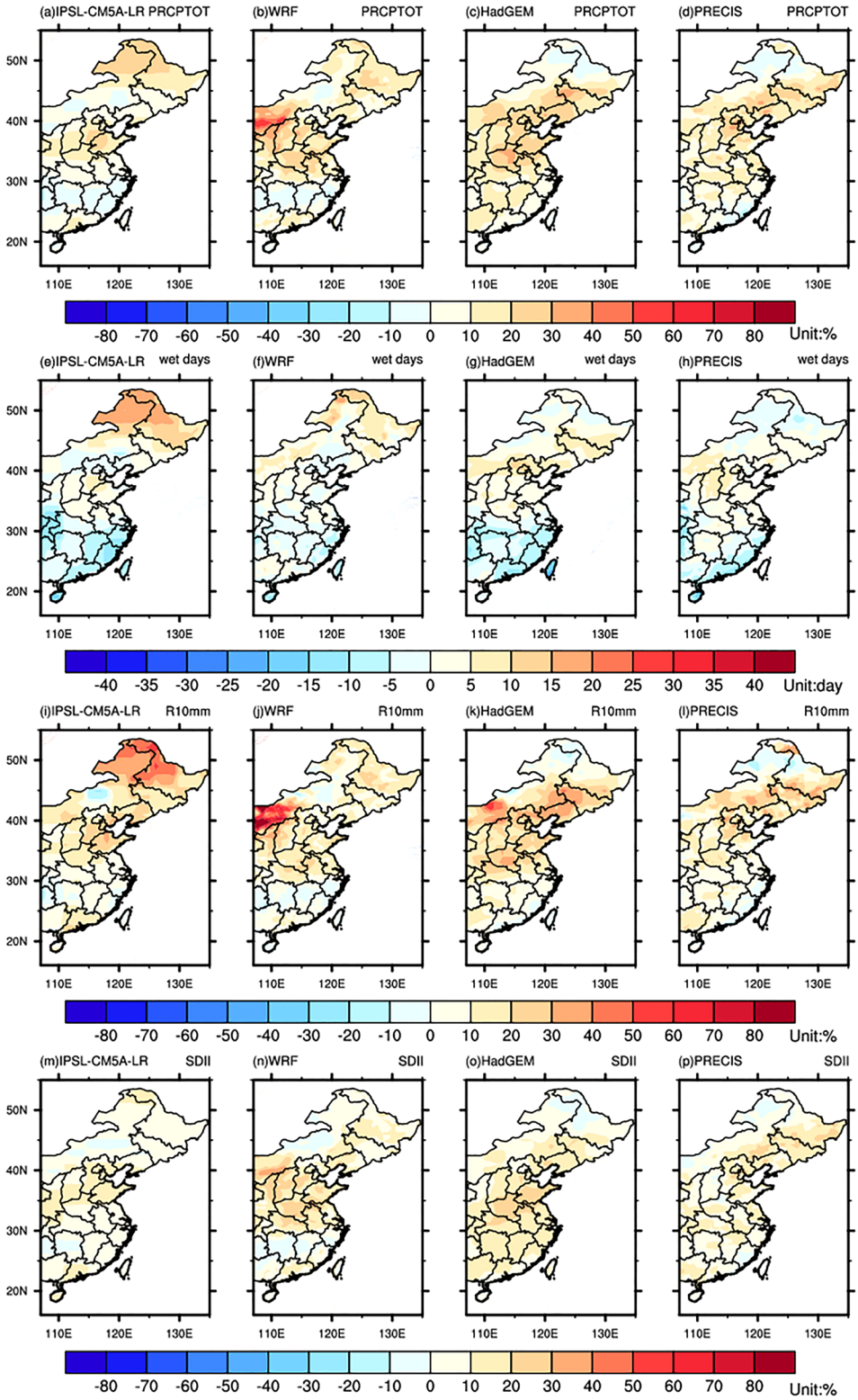

Figure 8. Changes in the annual mean state of precipitation indices between 2041–2060 and 1981–2000 under RCP8.5 scenario: PRCPTOT (a–d), number of wet days (e–h), R10mm (i–l), and SDII (m–p).

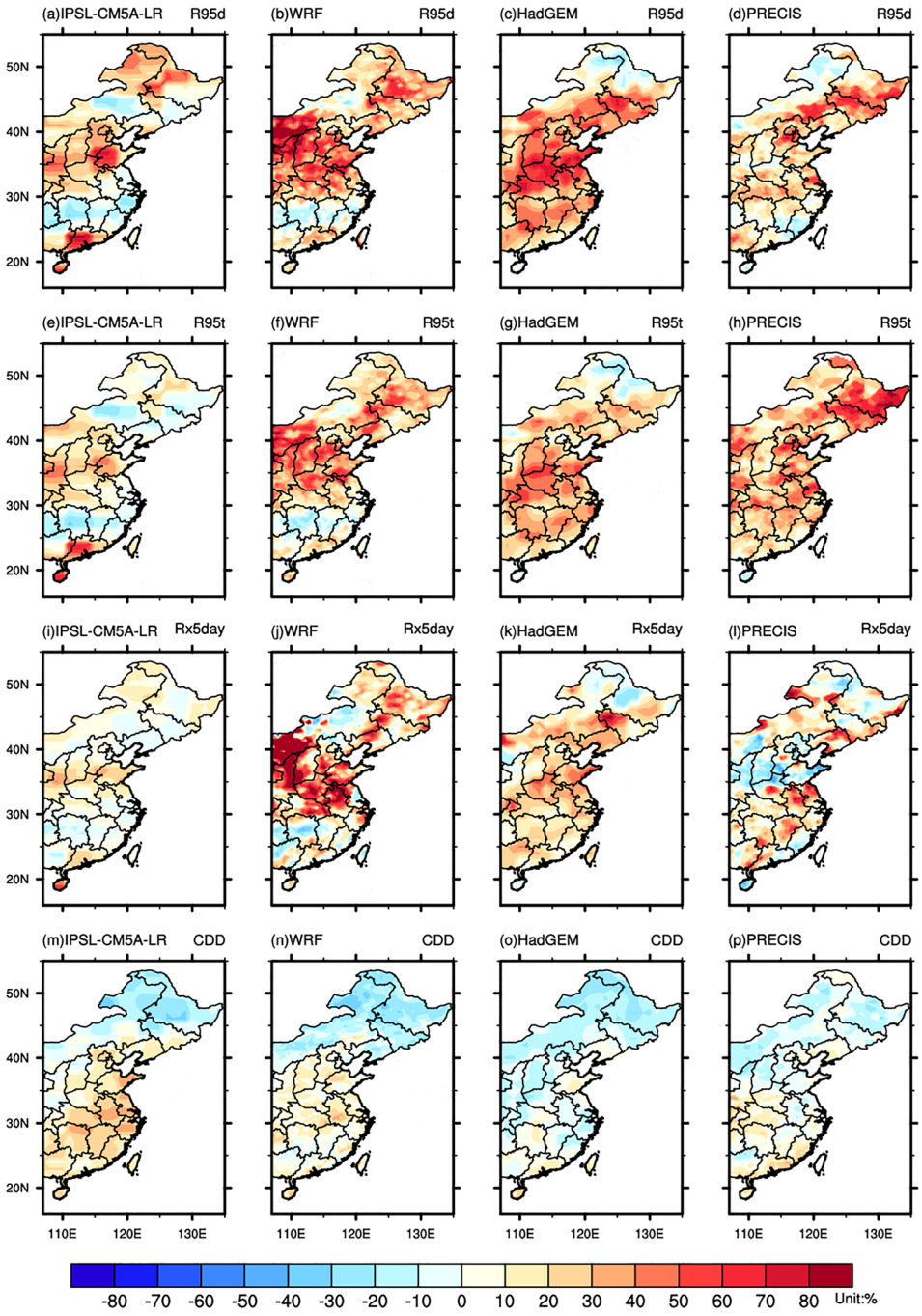

Figure 9. Changes in the annual mean state of precipitation indices between 2041–2060 and 1981–2000 under RCP8.5 scenario: R95d (a–d), R95t (e–h), Rx5day (i–l), and CDD (m–p).

produced by the same model (Figures 9e–9h). It is worth noting that the RCMs downscaling generally produce a stronger magnitude of R95t changes at regional scales compared with the driving GCMs. Bao et al. (2015) also projected a widespread increase of R95t over China by using WRF to downscale GFDL-ESM 2G. Rx5day is projected to increase in general, with the exceptions of slightly decreases in the southern and northeastern parts of the study region (Figures 9i–9l). The patterns of changes in Rx5day produced by RCMs are similar to those presented in Hui et al. (2018b), in which the authors use the RegCM4 and WRF to downscale the GCMs of EC-EARTH and IPSL-CM5A under the RCP8.5 scenario. For CDD

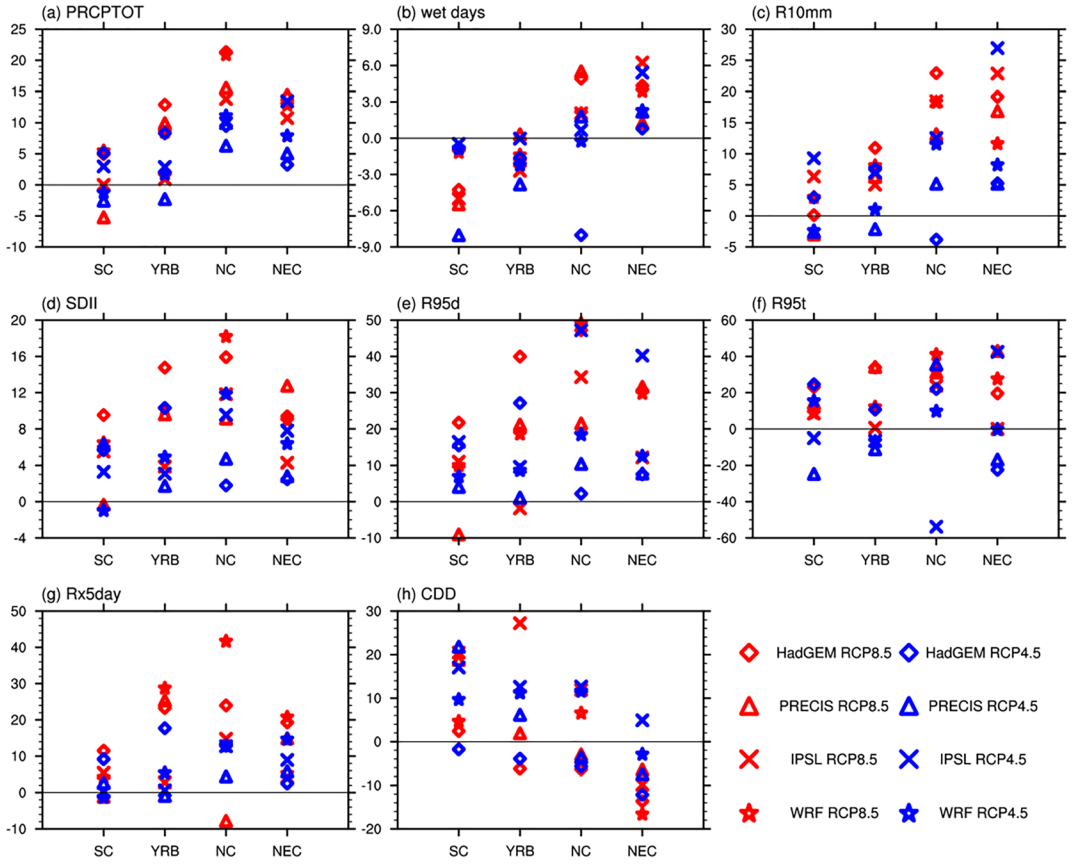

Figure 10. Projected changes (%) of precipitation indices averaged over subregions between 2041–2060 and 1981–2000 under RCP4.5 and RCP8.5 scenarios.

(Figures 9m–9p), all four models project decreases in north regions especially NEC, and three models (except HadGEM) project increases over south regions, with WRF and PRECIS showing weak changes in the southern areas.

Figure 10 summarizes the regional statistics for projected changes relative to the baseline period in indices of precipitation under RCP4.5 and RCP8.5 scenarios. Most markers in the figure are above the 0 line except the number of wet days over SC and YRB, and CDD over NC and NEC. This means a general increase in precipitation amount and intensity over Eastern China under both emission scenarios. A widespread increase of SDII is also reported in Zhu et al. (2018), which employed PRECIS to downscale HadGEM2-ES under the same RCP scenario. Results of R95t have the similar spatial distributions with R95d, but the decrease occurs more under RCP4.5. All models simulate positive changes of Rx5day in most subregions, and the magnitudes of average changes under RCP4.5 are generally lower than that under RCP8.5 (Figure 10g). As for the number of wet days and CDD, markers in Figures 10b and 10h suggest that the south subregions are very likely to have more dry days while NC and NEC are going to have more precipitation in 2041–2060.

5. Conclusion

In this study, we employ PRECIS and WRF, which are arguably two most influential RCMs, being driven by HadGEM2-ES and IPSL-CM5A, which are two GCMs from the Coupled Model Intercomparison Project Phase 5 (CMIP5), to investigate the impact of global warming on the characteristics of mean and extreme precipitations over Eastern China. We first evaluate the capacity of PRECIS and WRF as well as their driving GCMs in reproducing the historical climate of 1981–2000 and then use these four models to project mean and extreme precipitation over future warming climate of 2041–2060 under RCP4.5 and RCP8.5 scenarios.

Because of their improved resolution and better representation of finer-scale physical processes, WRF and PRECIS downscaling displays obvious advantages over their driving GCMs (IPSL and HadGEM, respectively) in the validation runs. For the mean climates, both RCMs are able to exhibit better annual precipitation measurements in terms of high correlations to observations, when downscaling IPSL-CM5A and HadGEM2-ES. Similar to other studies employing RCMs, the two RCMs show significant improvements over their forcing GCMs in terms of annual rainfall frequency and daily rainfall intensity of extreme rainfall events (Bao et al., 2015; Hui et al., 2018a; Zhu et al., 2018). Moreover, the two RCMs are able to capture the observed features of spatial distributions of extreme precipitation indices including V95p, R95t, and SDII, exhibiting higher spatial pattern correlations with observations than those of their driving GCMs. The two RCMs also produce more reasonable regional averages of extreme precipitation indices in most regions than their driving GCMs. Analysis in the supporting information further shows that PRECIS and WRF are able to better capture the temporal patterns of precipitation.

Under RCP4.5 and RCP8.5 scenarios, all four models project increasing annual precipitation over NEC, NC, and YRB regions. The four models also project that the daily precipitation intensity will increase over all the subregions of Eastern China. The results suggest that increased radiative forcing from RCP4.5 to RCP8.5 emission scenarios would add further strength to the daily precipitation intensity by 2041–2060. The projections indicate an increase in the values of extreme precipitation indices (SDII, R95d, and Rx5day) as well as in dry extreme index (CDD) over YRB and SC regions, meaning that these two regions will face the challenge of increasing floods and droughts in the future warming climate.

Owing to the ability of RCMs in representing finer-scale physical processes, PRECIS and WRF downscaling adds value in terms of present-day precipitation simulations with improved resolution and is able to produce more reliable projection results at the regional scale. However, it should be noted that large uncertainties still exist in future projections. First, PRECIS and WRF are driven by HadGEM and IPSL, respectively. To thoroughly attribute the difference of projections to the RCM itself or its driving GCM, the simulation of WRF or PRECIS driven by another GCM is needed, for example, PRECIS driven by IPSL-CM5A and WRF driven by HadGEM2-ES. Furthermore, multiple RCMs driven by multiple GCMs are needed so that projection uncertainty can be more comprehensively addressed. Second, a continuous run over the whole 21st century is need to fully cover the decadal variability. Third, the coupling of regional atmosphere model with an ocean model is needed to resolve the air-sea coupling process (Cabos et al., 2020). Fourth, for regional climate modeling, extreme climate indices are very sensitive to the choice of physical parameterization scheme; therefore, multiple physical parameterization scheme ensemble is also needed to fully cover the future climate change uncertainty.

Data Availability Statement

An archive of all the observed and model data sets used in this paper is presently available at The Open Science Framework (OSF) website (https://osf.io/74caq/).

Acknowledgments

This study was jointly supported by the National Key R&D Program of China (2018YFC1505601) and the National Natural Science Foundation of China (51761135024 and 41671113), UK-China Research and Innovation Partnership Fund through the Met Office Climate Science for Service Partnership (CSSP) China as part of the Newton Fund (AJYG-643BJQ), the Engineering and Physical Sciences Research Council of UK (R034214/1), the Netherlands Organization for Scientific Research (NWO) (ALWSD.2016.007), the High-level Special Funding of the Southern University of Science and Technology (Grants G02296302 and G02296402), and also Social Development Projects of STCSM (19DZ1201500 and 19DZ1201402). We thank Dr. Jia Wu from NCC of CMA and Dr. Xuejie Gao from Institute of Atmospheric Physics of Chinese Academy of Sciences for providing the CN05.1 gridded data set for model validation. We thank UK Met Office Hadley Centre for providing the HadGEM2-ES model output that we used to drive PRECIS. We thank Prof. Jianping Tang at Nanjing University for providing the output of regional climate model WRF. The authors also appreciate the support of Met Office Hadley Centre for providing regional climate model PRECIS.

References

Bao, J., & Feng, J. (2016). Intercomparison of CMIP5 simulations of summer precipitation, evaporation, and water vapor transport over Yellow and Yangtze River basins. *Theoretical and Applied Climatology*, *123*(3–4), 437–452. https://doi.org/10.1007/s00704-014-1349-y

Bao, J., Feng, J., & Wang, Y. (2015). Dynamical downscaling simulation and future projection of precipitation over China. *Journal of Geophysical Research: Atmospheres*, *120*, 8227–8243. https://doi.org/10.1002/2015JD023275

Bürger, G., Sobie, S., Cannon, A., Werner, A., & Murdock, T. (2013). Downscaling extremes: An intercomparison of multiple methods for future climate. *Journal of Climate*, *26*(10), 3429–3449. https://doi.org/10.1175/Jcli-D-12-00249.1

Cabos, W., de la Vara, A., Álvarez-García, F. J., Sánchez, E., Sieck, K., Pérez-Sanz, J. I., et al. (2020). Impact of ocean-atmosphere coupling on regional climate: The Iberian Peninsula case. *Climate Dynamics*, *54*, 4441–4467. https://doi.org/10.1007/s00382-020-05238-x

Chen, H. (2013). Projected change in extreme rainfall events in China by the end of the 21st century using CMIP5 models. *Chinese Science Bulletin*, *58*(12), 1462–1472. https://doi.org/10.1007/s11434-012-5612-2

Chen, L., & Frauenfeld, O. W. (2014). A comprehensive evaluation of precipitation simulations over China based on CMIP5 multimodel ensemble projections. *Journal of Geophysical Research: Atmospheres*, *119*, 5767–5786. https://doi.org/10.1002/2013JD021190

Chen, N., & Gao, X. (2019). Climate change in the twenty-first century over China: Projections by an RCM and the driving GCM. *Atmospheric and Oceanic Science Letters*, *12*(4), 270–277. https://doi.org/10.1080/16742834.2019.1612695

Chen, X., Xu, Y., & Yao, Y. (2015). Changes in climate extremes over China in a 2°C, 3°C, and 4°C warmer world. *Chinese Journal of Atmospheric Sciences*, *39*(6), 1123–1135. https://doi.org/10.3878/j.issn.1006-9895.1502.14224

Duan, W., Hanasaki, N., Shiogama, H., Chen, Y., Zou, S., Nover, D., et al. (2019). Evaluation and future projection of Chinese precipitation extremes using large ensemble high-resolution climate simulations. *Journal of Climate*, *32*(8), 2169–2183. https://doi.org/10.1175/jcli-d-18-0465.1

Easterling, D. R., Evans, J. L., Groisman, P. Y., Karl, T. R., Kunkel, K. E., & Ambenje, P. (2000). Observed variability and trends in extreme climate events: A brief review. *Bulletin of the American Meteorological Society*, *81*(3), 417–425. https://doi.org/10.1175/1520-0477(2000)081%3C0417:OVATIE%3E2.3.CO;2

Feng, J.-M., Wang, Y.-L., Ma, Z.-G., & Liu, Y.-H. (2012). Simulating the regional impacts of urbanization and anthropogenic heat release on climate across China. *Journal of Climate*, *25*(20), 7187–7203. https://doi.org/10.1175/JCLI-D-11-00333.1

Fu, G., Viney, N. R., Charles, S. P., & Liu, J. (2010). Long-term temporal variation of extreme rainfall events in Australia: 1910–2006. *Journal of Hydrometeorology*, *11*(4), 950–965. https://doi.org/10.1175/2010JHM1204.1

Gao, X., Shi, Y., Song, R., Giorgi, F., Wang, Y., & Zhang, D. (2008). Reduction of future monsoon precipitation over China: Comparison between a high resolution RCM simulation and the driving GCM. *Meteorology and Atmospheric Physics*, *100*(1–4), 73–86. https://doi.org/10.1007/s00703-008-0296-5

Gao, X., Shi, Y., Zhang, D., Wu, J., Giorgi, F., Ji, Z., & Wang, Y. (2012). Uncertainties in monsoon precipitation projections over China: Results from two high-resolution RCM simulations. *Climate Research*, *52*, 213–226. https://doi.org/10.3354/cr01084

Gao, X., Zongci, Z., & Giorgi, F. (2002). Changes of extreme events in regional climate simulations over East Asia. *Advances in Atmospheric Sciences*, *19*(5), 927–942. https://doi.org/10.1007/s00376-002-0056-2

Gao, X. J., Wang, M. L., & Filippo, G. (2013). Climate change over China in the 21st century as simulated by BCC_CSM1.1-RegCM4.0. *Atmospheric and Oceanic Science Letters*, *6*, 381–386. https://doi.org/10.3878/j.issn.1674-2834.13.0029

Ge, F., Zhu, S., Peng, T., Zhao, Y., Sielmann, F., Fraedrich, K., et al. (2019). Risks of precipitation extremes over Southeast Asia: Does 1.5 or 2 degrees global warming make a difference? *Environmental Research Letters*, *14*(4), 044015. https://doi.org/10.1088/1748-9326/aaff7e

Gemmer, M., Fischer, T., Jiang, T., Su, B., & Liu, L. L. (2011). Trends in precipitation extremes in the Zhujiang River basin, South China. *Journal of Climate*, *24*(3), 750–761. https://doi.org/10.1175/2010JCLI3717.1

Ghosh, A., Das, S., Ghosh, T., & Hazra, S. (2019). Risk of extreme events in delta environment: A case study of the Mahanadi delta. *Science of the Total Environment*, *664*, 713–723. https://doi.org/10.1016/j.scitotenv.2019.01.390

Hui, P., Tang, J., Wang, S., Niu, X., Zong, P., & Dong, X. (2018a). Climate change projections over China using regional climate models forced by two CMIP5 global models. Part I: evaluation of historical simulations. *International Journal of Climatology*, *38*, e57–e77. https://doi.org/10.1002/joc.5351

Hui, P., Tang, J., Wang, S., Niu, X., Zong, P., & Dong, X. (2018b). Climate change projections over China using regional climate models forced by two CMIP5 global models. Part II: projections of future climate. *International Journal of Climatology*, *38*, e78–e94.

IPCC (2012). Managing the risks of extreme events and disasters to advance climate change adaptation. In *A special report of working groups I and II of the intergovernmental panel on climate change* (pp. 1–582). Cambridge: Cambridge University press.

Jiang, Z., Li, W., Xu, J., & Li, L. (2015). Extreme precipitation indices over China in CMIP5 models. Part I: Model evaluation. *Journal of Climate*, *28*(21), 8603–8619. https://doi.org/10.1175/JCLI-D-15-0099.1

Jiang, Z., Song, J., Li, L., Chen, W., Wang, Z., & Wang, J. (2012). Extreme climate events in China: IPCC-AR4 model evaluation and projection. *Climatic Change*, *110*(1), 385–401. https://doi.org/10.1007/s10584-011-0090-0

Knutson, T. R., Sirutis, J. J., Vecchi, G. A., Garner, S., Zhao, M., Kim, H.-S., et al. (2013). Dynamical downscaling projections of twenty-first-century Atlantic hurricane activity: CMIP3 and CMIP5 model-based scenarios. *Journal of Climate*, *26*(17), 6591–6617. https://doi.org/10.1175/Jcli-D-12-00539.1

Lee, J.-W., Hong, S.-Y., Chang, E.-C., Suh, M.-S., & Kang, H.-S. (2014). Assessment of future climate change over East Asia due to the RCP scenarios downscaled by GRIMs-RMP. *Climate Dynamics*, *42*, 733–747. https://doi.org/10.1007/s00382-013-1841-6

Li, H., Chen, H., Wang, H., & Yu, E. (2018). Future precipitation changes over China under 1.5 degrees C and 2.0 degrees C global warming targets by using CORDEX regional climate models. *Science of the Total Environment*, *640-641*, 543–554. https://doi.org/10.1016/j.scitotenv.2018.05.324

Li, W., Jiang, Z., Xu, J., & Li, L. (2016). Extreme precipitation indices over China in CMIP5 models. Part II: Probabilistic projection. *Journal of Climate*, *29*(24), 8989–9004. https://doi.org/10.1175/JCLI-D-16-0377.1

Liang, Y., Wang, Y., Zhao, Y., Lu, Y., & Liu, X. (2019). Analysis and projection of flood hazards over China. *Water*, *11*(5), 1022. https://doi.org/10.3390/w11051022

Liu, J. W., Bo, L., Tian-Jun, Z., Xian-Feng, Z., & Lei, F. (2012). The extreme summer precipitation over East China during 1982–2007 simulated by the LASG/IAP regional climate model. *Atmospheric and Oceanic Science Letters*, *5*(1), 62–67. https://doi.org/10.1080/16742834.2012.11446966

Ma, S., Zhou, T., Dai, A., & Han, Z. (2015). Observed changes in the distributions of daily precipitation frequency and amount over China from 1960 to 2013. *Journal of Climate*, *28*(17), 6960–6978. https://doi.org/10.1175/JCLI-D-15-0011.1

Marengo, J. A., Tomasella, J., Alves, L. M., Soares, W. R., & Rodriguez, D. A. (2011). The drought of 2010 in the context of historical droughts in the Amazon region. *Geophysical Research Letters*, *38*, L12703. https://doi.org/10.1029/2011GL047436

Moore, B. J., Mahoney, K. M., Sukovich, E. M., Cifelli, R., & Hamill, T. M. (2015). Climatology and environmental characteristics of extreme precipitation events in the southeastern United States. *Monthly Weather Review*, *143*(3), 718–741. https://doi.org/10.1175/MWR-D-14-00065.1

Park, C., Min, S.-K., Lee, D., Cha, D.-H., Suh, M.-S., Kang, H.-S., et al. (2016). Evaluation of multiple regional climate models for summer climate extremes over East Asia. *Climate Dynamics*, *46*, 2469–2486. https://doi.org/10.1007/s00382-015-2713-z

Penalba, O. C., & Robledo, F. A. (2010). Spatial and temporal variability of the frequency of extreme daily rainfall regime in the La Plata Basin during the 20th century. *Climatic Change*, *98*, 531–550. https://doi.org/10.1007/s10584-009-9744-6

Pielke, R. A. Sr., & Wilby, R. L. (2012). Regional climate downscaling: What's the point? *Eos, Transactions American Geophysical Union*, *93*(5), 52–53. https://doi.org/10.1029/2012EO050008

Qin, P., & Xie, Z. (2016). Detecting changes in future precipitation extremes over eight river basins in China using RegCM4 downscaling. *Journal of Geophysical Research: Atmospheres*, *121*, 6802–6821. https://doi.org/10.1002/2016JD024776

Racherla, P. N., Shindell, D. T., & Faluvegi, G. S. (2012). The added value to global model projections of climate change by dynamical downscaling: A case study over the continental US using the GISS-ModelE2 and WRF models. *Journal of Geophysical Research*, *117*, D20118. https://doi.org/10.1029/2012JD018091

Shi, Y., Wang, G., & Gao, X. (2018). Role of resolution in regional climate change projections over China. *Climate Dynamics*, *51*, 2375–2396. https://doi.org/10.1007/s00382-017-4018-x

Shivam, G., Goyal, M. K., & Sarma, A. K. (2017). Index-based study of future precipitation changes over Subansiri river catchment under changing climate. *Journal of Environmental Informatics*, *34*, 1–14. https://doi.org/10.3808/jei201700376

Sillmann, J., Kharin, V., Zhang, X., Zwiers, F., & Bronaugh, D. (2013). Climate extremes indices in the CMIP5 multimodel ensemble: Part 1. Model evaluation in the present climate. *Journal of Geophysical Research: Atmospheres*, *118*, 1716–1733. https://doi.org/10.1002/jgrd.50203

Sillmann, J., Kharin, V. V., Zwiers, F., Zhang, X., & Bronaugh, D. (2013). Climate extremes indices in the CMIP5 multimodel ensemble: Part 2. Future climate projections. *Journal of Geophysical Research: Atmospheres*, *118*, 2473–2493. https://doi.org/10.1002/jgrd.50188

Singh, D., Tsiang, M., Rajaratnam, B., & Diffenbaugh, N. S. (2013). Precipitation extremes over the continental United States in a transient, high-resolution, ensemble climate model experiment. *Journal of Geophysical Research: Atmospheres*, *118*, 7063–7086. https://doi.org/10.1002/jgrd.50543

Sun, J., & Ao, J. (2013). Changes in precipitation and extreme precipitation in a warming environment in China. *Chinese Science Bulletin*, *58*(12), 1395–1401. https://doi.org/10.1007/s11434-012-5542-z

Tang, J., Niu, X., Wang, S., Gao, H., Wang, X., & Wu, J. (2016). Statistical downscaling and dynamical downscaling of regional climate in China: Present climate evaluations and future climate projections. *Journal of Geophysical Research: Atmospheres*, *121*, 2110–2129. https://doi.org/10.1002/2015jd023977

Taylor, K. E. (2001). Summarizing multiple aspects of model performance in a single diagram. *Journal of Geophysical Research*, *106*(D7), 7183–7192. https://doi.org/10.1029/2000JD900719

Wang, H.-J., Sun, J.-Q., Chen, H.-P., Zhu, Y.-L., Zhang, Y., Jiang, D.-B., et al. (2012). Extreme climate in China: Facts, simulation and projection. *Meteorologische Zeitschrift*, *21*(3), 279–304. https://doi.org/10.1127/0941-2948/2012/0330

Wang, X., Huang, G., Lin, Q., Nie, X., & Liu, J. (2015). High-resolution temperature and precipitation projections over Ontario, Canada: A coupled dynamical-statistical approach. *Quarterly Journal of the Royal Meteorological Society*, *141*(689), 1137–1146. https://doi.org/10.1002/qj.2421

Wang, X., Huang, G., & Liu, J. (2014). Projected increases in near-surface air temperature over Ontario, Canada: A regional climate modeling approach. *Climate Dynamics*, *45*, 1381–1393. https://doi.org/10.1007/s00382-014-2387-y

Wu, J., & Gao, X. J. (2013). A gridded daily observation dataset over China region and comparison with the other datasets. *Chinese Journal of Geophysics*, *56*, 1102–1111. https://doi.org/10.6038/cjg20130406 (in Chinese)

Wu, M., Luo, Y., Chen, F., & Wong, W. K. (2019). Observed link of extreme hourly precipitation changes to urbanization over coastal South China. *Journal of Applied Meteorology and Climatology*, *58*(8), 1799–1819. https://doi.org/10.1175/JAMC-D-18-0284.1

Xu, K., Xu, B., Ju, J., Wu, C., Dai, H., & Hu, B. X. (2019). Projection and uncertainty of precipitation extremes in the CMIP5 multimodel ensembles over nine major basins in China. *Atmospheric Research*, *226*, 122–137. https://doi.org/10.1016/j.atmosres.2019.04.018

Yang, T., Shao, Q., Hao, Z.-C., Chen, X., Zhang, Z., Xu, C.-Y., & Sun, L. (2010). Regional frequency analysis and spatio-temporal pattern characterization of rainfall extremes in the Pearl River Basin, China. *Journal of Hydrology*, *380*(3–4), 386–405. https://doi.org/10.1016/j.jhydrol.2009.11.013

You, Q., Kang, S., Aguilar, E., Pepin, N., Flügel, W.-A., Yan, Y., et al. (2011). Changes in daily climate extremes in China and their connection to the large scale atmospheric circulation during 1961–2003. *Climate Dynamics*, *36*, 2399–2417. https://doi.org/10.1007/s00382-009-0735-0

Yu, E., Sun, J., Chen, H., & Xiang, W. (2014). Evaluation of a high-resolution historical simulation over China: Climatology and extremes. *Climate Dynamics*, *45*, 2013–2031. https://doi.org/10.1007/s00382-014-2452-6

Yu, K., Hui, P., Zhou, W., & Tang, J. (2019). Evaluation of multi-RCM high-resolution hindcast over the CORDEX East Asia Phase II region: Mean, annual cycle and interannual variations. *International Journal of Climatology*.

Zhai, P., Zhang, X., Wan, H., & Pan, X. (2005). Trends in total precipitation and frequency of daily precipitation extremes over China. *Journal of Climate*, *18*(7), 1096–1108. https://doi.org/10.1175/JCLI-3318.1

Zhang, Q., Jiang, T., Chen, Y. D., & Chen, X. (2010). Changing properties of hydrological extremes in South China: Natural variations or human influences? *Hydrological Processes: An International Journal*, *24*(11), 1421–1432. https://doi.org/10.1002/hyp.7599

Zhou, B., Wen, Q. H., Xu, Y., Song, L., & Zhang, X. (2014). Projected changes in temperature and precipitation extremes in China by the CMIP5 multimodel ensembles. *Journal of Climate*, *27*(17), 6591–6611. https://doi.org/10.1175/JCLI-D-13-00761.1

Zhou, X., Huang, G. H., Baetz, B. W., Wang, X. Q., & Cheng, G. H. (2018). PRECIS-projected increases in temperature and precipitation over Canada. *Quarterly Journal of the Royal Meteorological Society*, *144*(711), 588–603. https://doi.org/10.1002/qj.3231

Zhu, J., Huang, G., Wang, X., Cheng, G., & Wu, Y. (2018). High-resolution projections of mean and extreme precipitations over China through PRECIS under RCPs. *Climate Dynamics*, *50*, 4037–4060. https://doi.org/10.1007/s00382-017-3860-1

Zou, L., & Zhou, T. (2013). Near future (2016-40) summer precipitation changes over China as projected by a regional climate model (RCM) under the RCP8. 5 emissions scenario: Comparison between RCM downscaling and the driving GCM. *Advances in Atmospheric Sciences*, *30*(3), 806–818. https://doi.org/10.1007/s00376-013-2209-x